

Transport of cold ions from the polar ionosphere to the plasma sheet

Kun Li,¹ S. Haaland,^{1,2} A. Eriksson,³ M. André,³ E. Engwall,³ Y. Wei,¹ E. A. Kronberg,¹ M. Fränz,¹ P. W. Daly,¹ H. Zhao,⁴ and Q. Y. Ren⁴

Received 20 February 2013; revised 7 August 2013; accepted 15 August 2013; published 6 September 2013.

[1] Ionospheric outflow is believed to be a significant contribution to the magnetospheric plasma population. Ions are extracted from the ionosphere and transported downtail by the large-scale convection motion driven by dayside reconnection. In this paper, we use a comprehensive data set of cold ion (total energy less than 70 eV) measurements combined with simultaneous observations from the solar wind to investigate the fate of these ions. By tracing the trajectories of the ions, we are able to find out where in the magnetotail ions end up. By sorting the observation according to geomagnetic activity and solar wind parameters, we then generate maps of the fate regions in the magnetotail and investigate the effects of these drivers. Our results suggest that, on overall, for about 85% of the cases, the outflowing ions are transported to the plasma sheet. The region where the ions are deposited into the plasma sheet is larger during geomagnetic quiet time than during disturbed conditions. A persistent dawn-dusk asymmetry in the plasma sheet deposition is also observed.

Citation: Li, K., et al. (2013), Transport of cold ions from the polar ionosphere to the plasma sheet, *J. Geophys. Res. Space Physics*, 118, 5467–5477, doi:10.1002/jgra.50518.

1. Introduction

[2] Every second, the Earth loses approximately 1 kg of mass in the form of ion outflow [Yau and Andre, 1997; Moore and Horwitz, 2007; Engwall et al., 2009a]. Ionospheric outflow is considered to be a significant or even dominant source of plasma supply to the terrestrial magnetosphere [e.g., Chappell et al., 1987; Moore and Horwitz, 2007]. This is corroborated by recent results by, e.g., André and Cully [2012] where it is shown that cold ions, i.e., ions with total energies below 70 eV, can sometimes dominate the number density in the near-Earth plasma environment.

[3] Ion outflow from the polar cap is closely associated with the polar wind [Axford, 1968; Banks and Holzer, 1968]. Electrons can escape from the polar ionosphere as photoelectrons and as a result of pressure gradients. As a consequence of escaping electrons, an ambipolar electric field is set up, which can accelerate light ions (H^+ and He^+) and cause them to escape the Earth's gravitational potential. Escape of light ions is modulated by solar irradiance (illustrated by Figure 9 in Engwall et al. [2009b]).

[4] There is also outflow from the cusp and cleft regions [e.g., Lockwood et al., 1985; Yau and Andre, 1997; Kistler et al., 2010] and the auroral region [Yau et al., 1985]. Outflow from these areas is mainly associated with ionosphere-magnetosphere coupling and is more strongly modulated by geomagnetic activity and solar wind energy input, which also allow heavier ions such as oxygen to escape.

[5] A significant part of the outflowing ions is directly lost downtail along open lobe field lines into the solar wind, but the majority is convected to the plasma sheet and thus recirculated within the magnetosphere [e.g., Cully et al., 2003; Haaland et al., 2012a], where they eventually contribute to the formation of the hot plasma sheet and ring current population [Kozyra, 1989; Moore and Horwitz, 2007; Cash et al., 2010]. Ion outflow possibly also plays a role for substorm triggering [e.g., Cully et al., 2003; Winglee and Harnett, 2011], although the role of ion outflow and its composition for substorm processes is still poorly understood.

[6] Obtaining reliable measurements of cold ions poses several challenges. In the polar cap and lobe regions of the terrestrial magnetosphere, the plasma density is very low and spacecraft charging effects will often prevent low-energy ions to reach particle detectors on a spacecraft. In the seminal paper by Chappell et al. [1987], where it was argued that the ionosphere alone was adequate to supply the magnetospheric plasma, the cold plasma population was referred to as “invisible” for this reason.

[7] Recent advances in instrumentation and techniques have allowed inclusion also of the *measured* contribution from cold plasma in ion outflow studies. In particular, the Cluster spacecraft quartet, with its comprehensive instrumentation, has provided more accurate measurements

¹Max-Planck Institute for Solar System Research, Katlenburg-Lindau, Germany.

²Birkeland Centre for Space Science, Department of Physics and Technology, University of Bergen, Bergen, Norway.

³Swedish Institute of Space Physics, Uppsala, Sweden.

⁴Beijing Institute of Spacecraft Environment Engineering, Beijing, China.

Corresponding author: K. Li, Max-Planck Institute for Solar System Research, Katlenburg-Lindau, Germany. (likun@mps.mpg.de)

of density [Pedersen *et al.*, 2001, 2008; Lybekk *et al.*, 2012], velocity, and flux of cold outflowing ions [Engwall *et al.*, 2006; Engwall *et al.*, 2009b] and convection [Förster *et al.*, 2007; Haaland *et al.*, 2007; Haaland *et al.*, 2008]. Results from these advances have shown that low-energy ions can dominate the density contribution in large regions of the Earth's magnetosphere. This has created a new awareness of the importance of cold plasma for the dynamics of the magnetosphere [Engwall *et al.*, 2009a; André and Cully, 2012].

[8] Cold ions are typically observed in the polar cap and lobe regions, as well as in the dayside magnetosphere. But observations suggest that cold ions can also be present along with hotter plasma in the plasma sheet [Seki *et al.*, 2003]. The origin of these ions is still debated though.

[9] Whereas there has been quite a lot of effort to understand the processes allowing the ions to escape, there has been less discussion about the fate of outflowing ions. Cully *et al.* [2003] investigated the role of cold ions supply to the plasma sheet. They used empirical models of the electric and magnetic fields combined with a simplified model of the ionospheric source population (a Monte Carlo simulation of approximately a test distribution with protons and oxygen ions with energies below 20 eV) and studied the transport from the ionosphere to the plasma sheet. By tracing the trajectories of the ions for various geomagnetic conditions and orientations of the interplanetary magnetic field (IMF), they were able to model the supply to the central plasma sheet. Their results showed that transport of thermal plasma between the ionosphere and the central plasma sheet is largely governed by the convection electric field. Later, Ebihara *et al.* [2006] employed empirical models of the O⁺ distribution combined with models of the electric and magnetic fields to investigate the fate of suprathermal oxygen. Their results suggested greatly enhanced feed to the inner parts of the magnetosphere during active geomagnetic conditions.

[10] In this paper, which is a follow-up of the work published by Li *et al.* [2012] and a more concise treatment of the discussion in Haaland *et al.* [2012a, 2012b], rather than using a model distribution as done in, e.g., Cully *et al.* [2003] and Ebihara *et al.* [2006], we use in situ measurements of cold ions obtained from the Cluster spacecraft. Also, instead of using simple relations between convection and transport as done in Haaland *et al.* [2012a, 2012b], we here do a full particle tracing to determine the trajectory and fate of each individual ion. By utilizing a large data set, we are thus able to generate maps of the cold ion supply to the plasma sheet and investigate how the intensity and spatial distribution of the ion supply to the plasma sheet are affected by solar wind condition and geomagnetic disturbance level.

2. Cold Ion Outflow Measurements

[11] The primary database for this study is the cold ion data set from Engwall *et al.* [2009b], and later used in, e.g., Haaland *et al.* [2012a], Li *et al.* [2012], and Haaland *et al.* [2012b]. This data set contains approximately 180,000 records with cold plasma density, velocity, and flux, together with auxiliary data such as geomagnetic activity indices and solar wind parameters. The solar wind data are OMNI2

data with source from ACE and WIND spacecraft in 1 h resolution [King and Papitashvili, 2005].

[12] Below, we provide a brief motivation for using this data set and a short description of the methodology. For more details about the technique, coverage, error estimation, and data set characteristics, we refer to the original publications by Engwall *et al.* [2006] and Engwall *et al.* [2009a, 2009b].

2.1. Spacecraft Charging

[13] Transport of plasma from the high altitude ionosphere to the central plasma sheet takes place through the polar cap and magnetotail lobe regions. These are regions characterized by a very tenuous plasma. A sunlit, conductive spacecraft immersed in this plasma will attain a positive potential relative to the ambient plasma. This potential is primarily governed by solar irradiation in the extreme ultraviolet (EUV) range causing emission of photoelectrons from the spacecraft surface. As a consequence, ions with energies below the spacecraft potential energies will not be able to reach the spacecraft. Likewise, electron detectors onboard the spacecraft may get contaminated by the emitted photoelectrons. Moment calculations based on particle instruments will therefore not be reliable.

[14] Spacecraft charging and effects thereof can be reduced by actively controlling the spacecraft potential, typically by emitting heavy ions to counterbalance the photoemission of electrons. This technique, using ion emitters, was installed on many previous missions, e.g., the Geotail [Schmidt *et al.*, 1995; Riedler *et al.*, 1997], POLAR [Moore *et al.*, 1995], Equator-S [Torkar *et al.*, 1999], Interball [Riedler *et al.*, 1998], and is also used in the more recent missions such as Double-Star and Cluster [Torkar *et al.*, 2001]. Although it is typically not possible to bring and keep the spacecraft to zero potential, the technique can provide significant improvements in plasma measurements.

[15] One example of a successful use of active spacecraft voltage control for the purpose of measuring cold ion outflow was the study by Su *et al.* [1998a]. They used ion moments from the Thermal Ion Dynamics Experiment onboard the POLAR spacecraft. For a limited time period (April and May 1996) when the Plasma Source Instrument [see Moore *et al.*, 1995, 1997] was operating, the spacecraft could be stabilized to a potential around 2 V above the ambient plasma.

[16] Due to the above spacecraft charging issue, but also other limitations in the instrumentation and measurement techniques, many of the earlier observations of ion outflow at high altitudes still only contained measurements of ions with energies above a certain threshold.

2.2. Cold Ion Density and Velocity

[17] The negative effect of spacecraft charging discussed above can be turned to an advantage, and the Engwall *et al.* [2009a] data set, which forms the backbone of the present study, utilizes spacecraft potential to derive both density and velocity of cold ions.

[18] For a given solar irradiance, and knowledge about spacecraft surface properties such as conductivity and total area, the spacecraft potential can be used to derive the ambient electron density, N_e , from a simple relation:

$$N_e \sim A e^{-V_s/B} \quad (1)$$

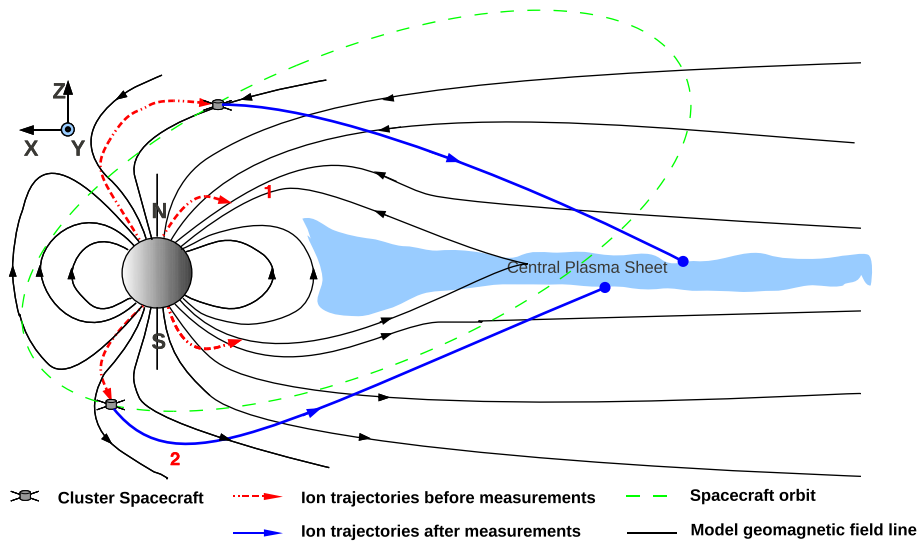


Figure 1. Schematic diagram showing the tracing procedure. Starting at the location of Cluster, the trajectories of the ions are calculated using the guiding center of motion. The landing point is $1 R_E$ away from the neutral sheet to avoid the sharp gradients and nonadiabatic motion in the central plasma sheet.

where the coefficients A and B depend on spacecraft properties and solar irradiance. The spacecraft voltage, V_s is typically obtained from double probe electric field measurements. Assuming quasi neutrality and singly charged ions, the ion density is identical to the electron density.

[19] Several studies have utilized this relation to estimate plasma densities in the magnetosphere [e.g., Pedersen, 1995; Pedersen *et al.*, 2001; Escoubet *et al.*, 1997; Laakso *et al.*, 1997; Scudder *et al.*, 2000]. More accurate density determination from this method has become available from Cluster observations. Pedersen *et al.* [2008] and later Engwall *et al.* [2009a, 2009b] and Lybekk *et al.* [2012] made use of measurements from the Electric Field and Wave instrument (EFW) [see Gustafsson *et al.*, 2001] combined with solar extreme ultraviolet observations and a model of the potential distribution around the spacecraft [Cully, 2007] to obtain calibrated density values for the polar cap and lobe regions.

[20] A novel combination of spacecraft potential and two complementing electric field measurement techniques also makes it possible to calculate the velocity of the cold ions [Engwall *et al.*, 2006, 2009a, 2009b]. In a cold tenuous plasma, the spacecraft potential energy will typically exceed the bulk kinetic energy of the ions. If, in addition, the thermal energy is lower than both these values, the following inequality holds:

$$kT_i < E_k < eV_{sc} \quad (2)$$

where k is the Boltzmann constant, T_i is the ion temperature, E_k is the bulk energy of the ions, and eV_{sc} is the potential energy of the spacecraft.

[21] As a consequence of the above inequality, a wake void of ions forms behind the spacecraft [see, e.g., Eriksson *et al.*, 2006]. The far more mobile electrons, on the other hand, will be able to fill the wake. Consequently, the EFW instrument will detect an electrostatic field in the direction of the wake.

[22] Cluster also provides very precise convection measurements from the Electric Drift Instrument (EDI) [see,

e.g., Paschmann *et al.*, 2001]. EDI emits a 1 keV electron beam and measures the gyro-center displacement and gyration time of the emitted electrons. For a given magnetic field (which can be determined from the gyration time), the gyro-center displacement can then be used to calculate the convection electric field. Since the gyroradii of these ions are much larger than the typical-scale size of the wake, EDI measurements are not affected by the wake.

[23] By combining the convection electric field, the wake electric field, and the magnetic field orientation, it is thus possible to calculate the parallel outflow velocity of the cold ions. In general, higher convection velocities and higher wake electric fields will give a more reliable determination of the parallel velocity. To ensure sufficiently accurate results, cases where the convection velocity was below 0.8 km s^{-1} have been discarded in the cold ion data set. One should therefore have in mind that the data set is slightly biased toward periods with high convection and thus to periods with moderate to disturbed magnetospheric conditions. Cases with F10.7 index below $100 \times 10^{-22} \text{ W} \cdot \text{s} \cdot \text{m}^{-2}$ were also discarded, since low solar irradiance prevented plasma wake. For more details about the underlying assumptions, methodology, and error bounds of this technique, we refer to the papers by Eriksson *et al.* [2006] and Engwall *et al.* [2009b].

3. Tracing Methodology

[24] Our measurements of cold ions are taken in the polar cap and lobe regions at geocentric distances between 4 and 19 Earth radii (R_E). To determine the fate of the ions, we trace each individual observation to the edge of the plasma sheet (i.e., $1 R_E$ above the central plasma sheet), as illustrated in Figure 1. For this purpose, we use the first-order guiding center equation of motion as described in Northrop [1963]:

$$m \frac{dV_{\parallel}}{dt} = m \vec{V}_{\vec{E} \times \vec{B}} \cdot \frac{d\hat{b}}{dt} + mg_{\parallel} - eE_{\parallel} - \frac{\mu}{m} \frac{\partial B}{\partial S} \quad (3)$$

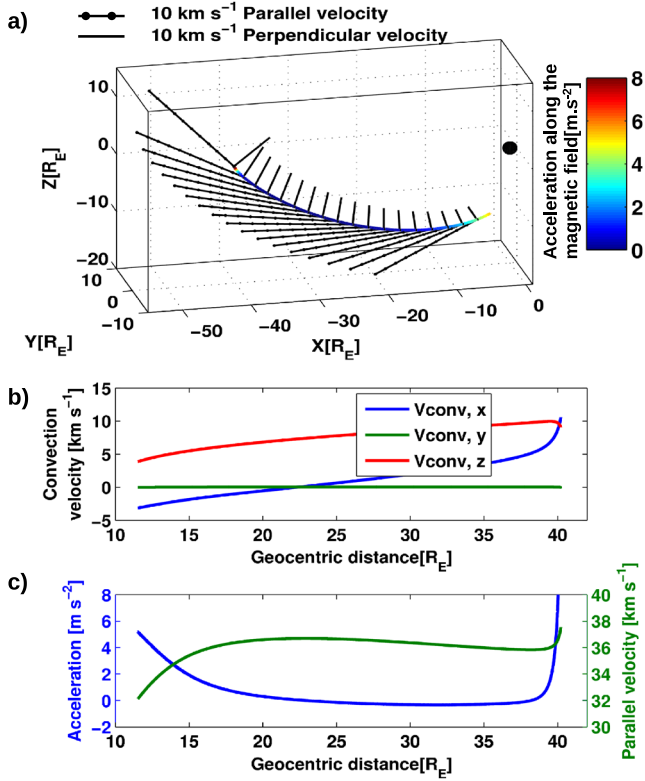


Figure 2. Trajectory of a cold ion measured by Cluster at $[-2.9, -0.1, -11.1] R_{EGSM}$ in the Southern Hemisphere. (a) B_{IMF} was $[-7.2, 0.6, 2.4] \text{ nT}_{GSE}$, and solar wind dynamic pressure was 2.08 nPa during this event. During the 120 min it takes for the ion to travel from the spacecraft position to the plasma sheet, parallel velocity (c), convection velocity (b), and acceleration (c) change. In this case, the landing point was traced to the position $[-40.2, -0.1, 0.4] R_{EGSM}$ in the plasma sheet.

where V_{\parallel} is the parallel velocity, $\vec{V}_{\vec{E} \times \vec{B}}$ is the convection velocity, m is the ion mass (i.e., proton mass), \hat{b} is a unit vector along the magnetic field, g_{\parallel} is the component of gravity along the magnetic field, e is the elementary charge, E_{\parallel} is the magnetic field aligned electric field, μ is the magnetic moment of the ion, and S is the length of line along the magnetic field.

[25] Not all of the above terms are relevant in the polar cap and lobe regions. The mirror force is only relevant where there are strong gradients in the magnetic field and/or the particles have a large magnetic moment. Since the magnetic field lines are assumed to be equipotential, there will also be no acceleration due to parallel electric fields, although the significance of field aligned potential drop along open field lines is debated [e.g., *Fairfield et al.*, 2008; *Winningham and Gurgiolo*, 1982; *Horwitz et al.*, 1992; *Wilson et al.*, 1997; *Su et al.*, 1998b].

[26] In effect, only the centrifugal acceleration [e.g., *Cladis*, 1986] is relevant for the present study, i.e., tracing the ions from the high latitude polar cap region to the plasma sheet. An assessment of the role of centrifugal acceleration of cold ions was done by *Nilsson et al.* [2008, 2010]. They found that although the centrifugal acceleration were mostly

small—typical values were only a few ms^{-2} —the large travel distances involved can lead to a significant increase in parallel velocity of the ions between the point of observation and a target point far downtail. Acceleration is also apparent in *Engwall et al.* [2009a]; the observed parallel velocities are in general higher at large radial distances (near Cluster apogee around $19 R_E$) than closer to Earth.

[27] For the actual tracing, we proceed as follows: For a given time, t_0 , we start tracing from the spacecraft location, where parallel velocity and acceleration as well as convection and the magnetic field are known (measured). The convection electric field, \vec{E}_{sc} , measured at the spacecraft enters the convection by $\vec{V}_{\perp,sc} = \vec{E}_{sc} \times \vec{B}_{sc} / B_{sc}^2$. The convection is along the magnetic tension force, $(\vec{B}_i \cdot \nabla) \vec{B}_i$. These values are then used to calculate subsequent values at a position r_1 , time t_1 , 2 s later. Here we have used the magnetic field model and scaled the convection velocity along the magnetic flux tube, assuming flux tube conservation. For density estimation at the new position, we assume particle flux conservation along the magnetic flux tube. This scheme is repeated, and in general, at a position r_i and time t_i , we then have the following parallel velocity, convection, and flux:

$$\vec{V}_{\parallel,i} = \vec{V}_{\parallel,i-1} + \frac{dV_{\parallel}}{dt} \Delta t \quad (4)$$

$$\vec{V}_{\perp,i} = |\vec{V}_{\perp,sc}| \sqrt{\frac{|\vec{B}_{sc}|}{|\vec{B}_i|}} \left(\frac{(\vec{B}_i \cdot \nabla) \vec{B}_i}{|(\vec{B}_i \cdot \nabla) \vec{B}_i|} \right) \quad (5)$$

$$j_i = n_{sc} V_{\parallel,sc} \frac{|\vec{B}_i|}{|\vec{B}_{sc}|} \quad (6)$$

In these equations, \vec{B}_{sc} is the magnetic field measured by spacecraft at time t_0 , \vec{B}_i is the magnetic field value from the model [*Tsyganenko*, 2002a, 2002b] at time t_i but parameterized with the solar wind, IMF, and geomagnetic activity indices for time t_0 .

[28] The landing point of the ions was defined to be $1 R_E$ away from the neutral sheet, i.e., where the model B_x changes sign (which in general is different from $Z_{GSM} = 0$). The $1 R_E$ is somewhat arbitrary, but closer to the field reversal region, inside the central plasma sheet, our assumption that centrifugal acceleration is the only relevant force is probably violated. Also, the sharp gradients in the magnetic field near the neutral sheet may cause nonadiabatic acceleration and hence a breakdown of the guiding center approximation [*Cully et al.*, 2003].

[29] Figure 2 shows an example of an ion observed by Cluster at $r_i = [-2.9, -0.1, -11.1] R_{EGSM}$. The initial parallel velocity is around 32 km s^{-1} , and the convection velocity is around 5 km s^{-1} . As the ion travels downtail, it is exposed to both parallel acceleration as a result of centrifugal forces, and perpendicular acceleration due to increase in the convection velocity as the flux tube expands. After approximately 120 min, the ion reaches the landing point $1 R_E$ below the neutral sheet in this case.

[30] Due to the Cluster orbit, Southern Hemisphere observations are on average taken at higher altitudes and with better dayside coverage than the corresponding northern hemisphere observations [see *Li et al.*, 2012 for details]. In the following, we have therefore treated Northern and Southern Hemispheres observations separately.

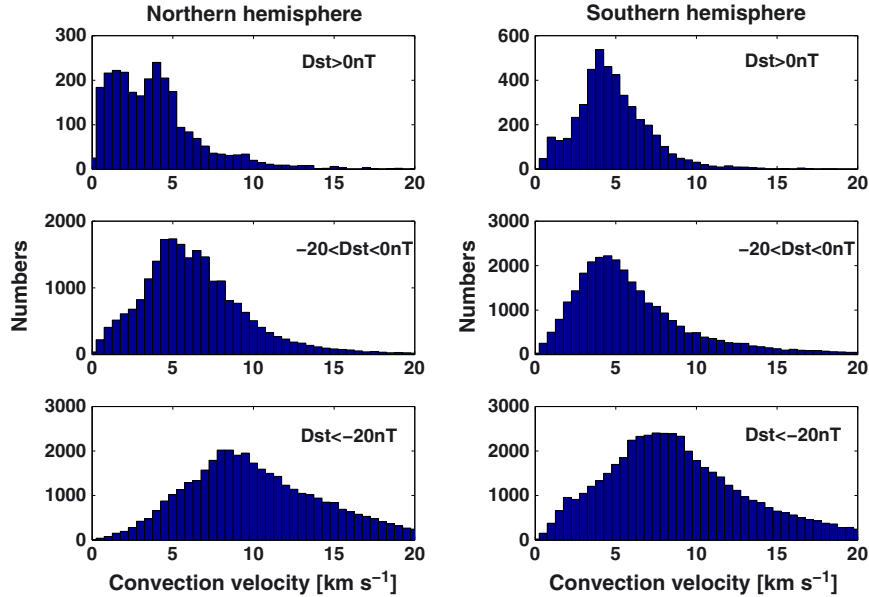


Figure 3. Distribution of observed convection velocities for three different geomagnetic activity levels.

4. Supply of Cold Ions to the Plasma Sheet

[31] The *Engwall et al.* [2009b] data set consist of a total of 172,817 records with cold ion velocity and density. Of these, we were able to trace 146,874 ion trajectories to the plasma sheet (64,457 and 82,417 cases from the Northern and Southern Hemispheres, respectively). For the remaining cases, the trajectories either lead to the magnetopause or suggested landing points outside the magnetic field model limits.

[32] The large number of observations allow us to create subsets of the data and generate maps of the landing regions in the magnetotail. In order to examine the role of the interplanetary magnetic field or geomagnetic activity as driver parameters, we extracted data containing only within certain ranges of these driver parameters (detailed in sections 4.2 and 4.3).

[33] In the following, we have chosen to present the plasma sheet feed in the form of maps of $2 \times 2 R_{EGSM}^2$ resolution, where the average (arithmetic mean) flux in each pixel is represented by colors. To ensure sufficient reliability in the averages, we require a minimum of N individual values in each bin. The value N is given by

$$N = 40 \times N_I / N_T \quad (7)$$

where N_T is the total number of observations (146,874) and N_I is the number of observations in each subset. Typical values of N in the maps are 10–20; regions with less than $N = 3$ are always discarded.

4.1. Transport of Cold Ions to the Plasma Sheet

[34] Earlier results [e.g., *Cully et al.*, 2003] have demonstrated that the cold ion trajectories are primarily controlled by the convection (and the magnetic field topology). As explained in section 2.2, the convection measurements in the *Engwall et al.* [2009b] data set are biased toward high convection velocities. Consequently, the average convection

velocity in each subset will be too high. To compensate for this, we therefore recalibrate the convection velocity. The calibration is done by multiplying each measured convection velocity with a scaling factor to ensure that each subset has the same average as the unbiased data set of *Haaland et al.* [2008]. Whereas there are large variations in the convection velocities, neither outflow flux nor parallel velocities of the ions vary much with geomagnetic activity.

[35] Figure 3 shows the distribution of convection velocities for each disturbance level range for the Northern and Southern Hemispheres, respectively. The distribution are highly non-Gaussian, so the statistical moments, mean, median, and mode are very different. All panels show a clear shift toward higher convection velocities during disturbed conditions though.

[36] The large spread in convection velocities in our data set will also cause a correspondingly large spread in the travel times of the ions. The fastest ions, starting out in the nightside during disturbed condition and high convection, only use around 30 min to reach the plasma sheet. The longest transport times, typically ions starting out on the day-side and during periods with low convection, were found to be more than 5 h.

[37] Our data set does not contain any periods with extreme solar wind or geomagnetic conditions. The magnetic field topology, given by the Tsyganenko T01 model, therefore does not vary much in the regions relevant for this study (polar cap and lobes). Still, the topology plays a role since it determines the direction of convection.

[38] Figure 4 shows example of the magnetic topology and average travel time for two different levels of geomagnetic activity. During quiet conditions (top), the convection velocity is typically low (see Figure 3) and with a tailward component (the Z_{GSM} component of the convection velocity is still dominant, but there is also a negative X_{GSM} component) at high latitudes inside approximately $28 R_E$ in the figure. As a result, average transport times will be large

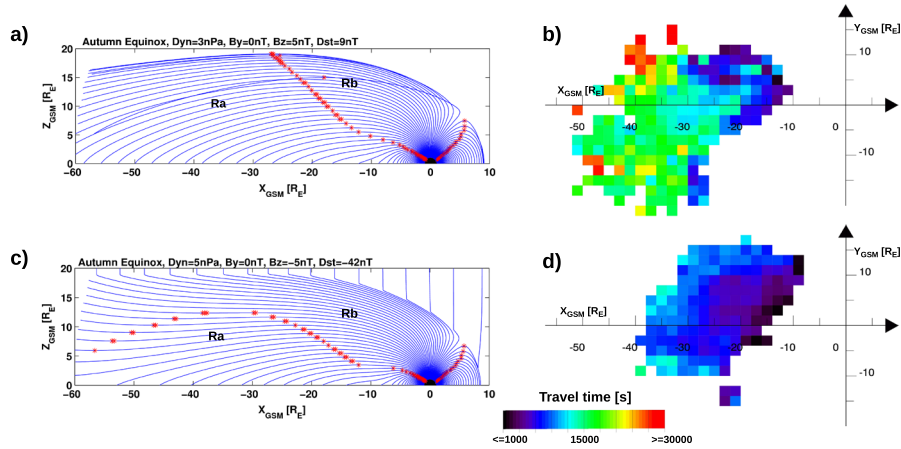


Figure 4. Magnetic field topology (left) and cold ion transport times (right). (a) XZ_{GSM} projection of the magnetic topology obtained from the Tsyganenko T01 magnetic field model during quiet conditions. The convection is low, predominantly in Z_{GSM} direction, but with nonnegligible components in X_{GSM} direction. The red stars mark the separation between earthward convection (positive X_{GSM} —marked Ra) and tailward convection (negative X_{GSM} —marked Rb). (b) Color-coded map of the plasma sheet. Colors indicate transport time from the northern polar cap ionosphere to the plasma sheet during quiet geomagnetic conditions. Each pixel shown is the average of minimum $N = 3$ individual values. (c) Same as Figure 4a but for disturbed magnetospheric conditions. The field topology is now more stretched, and the convection is predominantly in the Z_{GSM} direction. (d) Map of transport times for disturbed conditions. Due to the higher convection velocity, the transport times are much lower than for quiet conditions.

(typically 5 h) and cause a deposition of the outflowing ions over a large region of the tail. A significant amount of the ions end up tailward of $35 R_E$.

[39] During disturbed conditions (bottom), the convection is higher and with a more stretched field line topology that implies a convection essentially in the Z_{GSM} direction, i.e., fast convection toward the plasma sheet. The average transport times between the ionosphere and the plasma sheet is much lower (156 min).

[40] During the long transport times, there will inevitably be some fluctuations in solar wind parameters, convection, and magnetic field topology. Since our observations are not continuous in time, and we use a static magnetic field model, we are presently not able to assess the effect of such fluctuations, though.

4.2. Response to Geomagnetic Activity

[41] In order to investigate how the transport of cold ions are influenced by geomagnetic activity, we sorted the data according to the Disturbed Storm Time (Dst) index. The Dst index is a proxy for global magnetospheric storm activity and primarily indicates the intensity of the Earth's ring current. Due to the long transport times involved in ion outflow, the Dst index is more suitable than, e.g., the frequently used Auroral Electrojet (AE) index. (There is often a high degree of mutual correlation between solar wind parameters and the AE and Dst indices, however [e.g., Förster *et al.*, 2007].) Sorting according to Dst values also enables us to directly compare the present results with the source region tracing in Li *et al.* [2012] and the cold ion loss versus circulation discussion by Haaland *et al.* [2012a].

[42] Quiet magnetospheric conditions and positive or small negative Dst values are typically associated with northward IMF conditions and low and stagnant convection.

Correspondingly, disturbed conditions (in our paper defined as Dst values below -20 nT to ensure sufficient statistics) are typically associated with southward IMF, dayside reconnection, and high convection.

[43] The resulting maps for the Northern Hemisphere are shown in the right panels of Figure 5. Each row in this figure represents a certain Dst range, starting with quiet conditions on the top, thereafter intermediate geomagnetic activity and disturbed conditions in the bottom.

[44] For convenience, we also reproduce the ionospheric source maps from Li *et al.* [2012] in the left panels of this figure. The source maps are projected into an altitude corrected geomagnetic coordinate system [see Baker and Wing, 1989], and each pixel covers an approximately $65,000 \text{ km}^2$ area at 1000 km altitude of the polar cap ionosphere. Note that the color scales for the source maps and plasma sheet maps have different ranges.

[45] The corresponding maps for Southern Hemisphere are shown in Figure 6. Table 1 provides additional details about these figures.

[46] In general, quiet conditions are characterized by a contracted polar cap region and low fluxes. Tracing to the plasma sheet suggests a large spread across the tail where a substantial amount of the outflowing cold ions end up tailward of $55 R_E$ downtail. This is particularly apparent in the Southern Hemisphere and can be explained by low convection velocity which allows the ions to travel further downtail before reaching the plasma sheet. The average transport times from the ionosphere to the plasma sheet are 243 and 342 min for the Northern and Southern Hemispheres, respectively.

[47] During moderate conditions, the average convection velocity is higher, whereas the parallel velocities do not change very much. As a result, the outflowing ions are

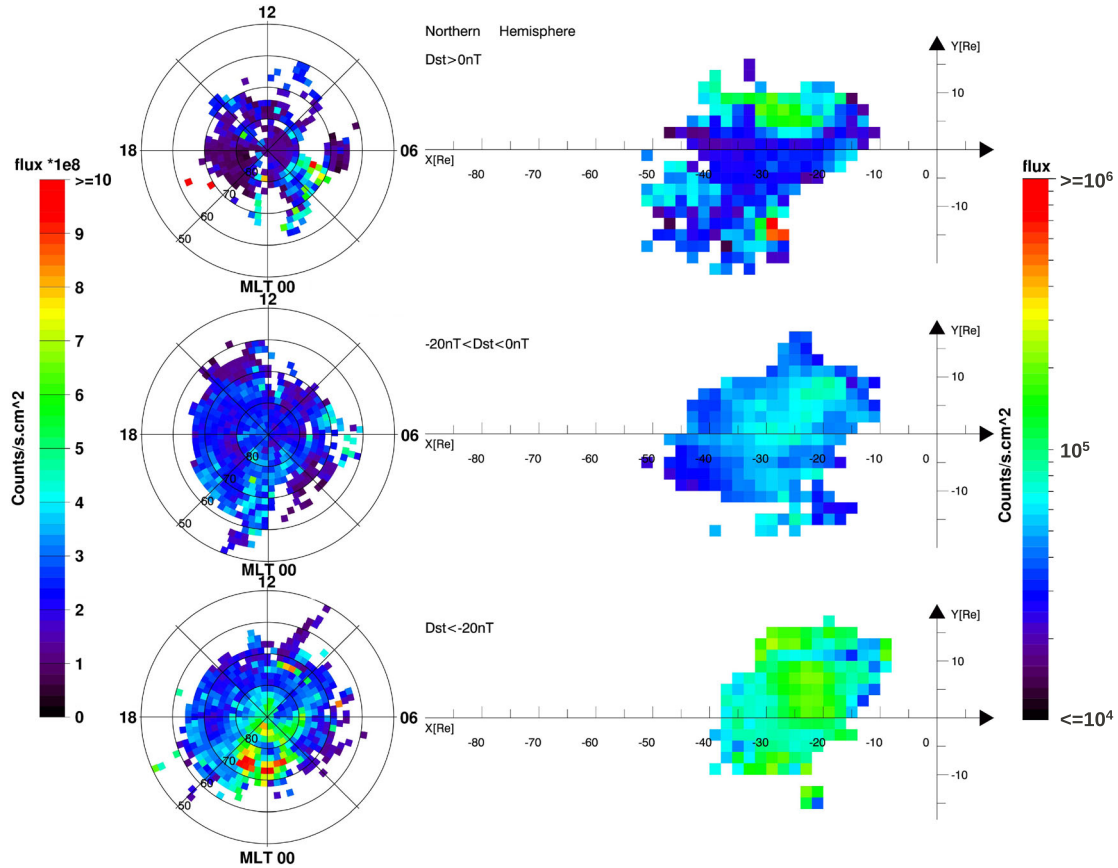


Figure 5. Maps of cold ion source regions in the Northern Hemisphere polar cap region (left) and the corresponding landing regions in the plasma sheet (right) for different levels of geomagnetic activity. (Top) Quiet geomagnetic conditions, typically associated with low convection. The polar cap region is contracted, the outflow flux is low, and the outflowing ions are distributed over a fairly large region rather far downtail in the magnetotail. The average travel time from the ionosphere to the plasma sheet is around 243 min. (Center) Moderate geomagnetic activity levels. The polar cap is now more expanded, and the overall outflow is higher. Since the convection is higher, the cold ions are transported faster to the plasma sheet and end up closer to the Earth. The average travel time from the ionosphere to the plasma sheet is 204 min. (Bottom) Disturbed magnetospheric conditions, typically associated with a stretched magnetic topology, and high convection. The ionospheric outflow is higher, and the high convection velocity causes the ions to be deposited closer to the Earth. The average transport time is around 156 min.

transported faster to the plasma sheet. Although the polar cap is more expanded, and the total outflow is larger, the ions end up closer to the Earth than during quiet conditions. The average transport times are 204 and 326 min for the Northern and Southern Hemispheres, respectively.

[48] During disturbed conditions, we observe an even more expanded polar cap region with higher outflow rates. As pointed out by *Li et al.* [2012], we also observe elevated outflow from the cusp and auroral regions (due to the Cluster orbit, the auroral zone is primarily observed in the Northern Hemisphere, whereas the cusp is primarily observed in the Southern Hemisphere. We refer to *Li et al.* [2012] for further details here). Due to the high convection velocity, the outflowing cold ions are rapidly transported to the plasma sheet and essentially, no ions are able to escape tailward of $55 R_E$. Mean transport times are 156 and 252 min for the Northern and Southern Hemispheres, respectively.

[49] Figure 6 shows the corresponding maps for the Southern Hemisphere. The overall pattern is the same

as for the Northern Hemisphere: a contracted polar cap area and a distribution of the cold ions to positions far downtail during quiet conditions and an expanded polar cap and fast transport to regions closer to Earth during disturbed conditions.

[50] As demonstrated in Figure 4 and the maps in Figures 5 and 6, the transport times and landing regions are largely controlled by the convection velocity. Whereas the convection can vary from essentially zero to several tens of kilometers per second, the parallel outflow velocity does not change that much with geomagnetic activity [see, e.g., Figures 6 and 8 in *Engwall et al.*, 2009b]. As a consequence, quiet conditions and low convection will cause the outflowing ions to be deposited further downtail than during disturbed condition. They will therefore spend more time in the magnetotail where they are exposed to various acceleration mechanisms. By the same taken, ions supplied closer to the Earth will spend less time in the magnetotail and potentially undergo less energization.

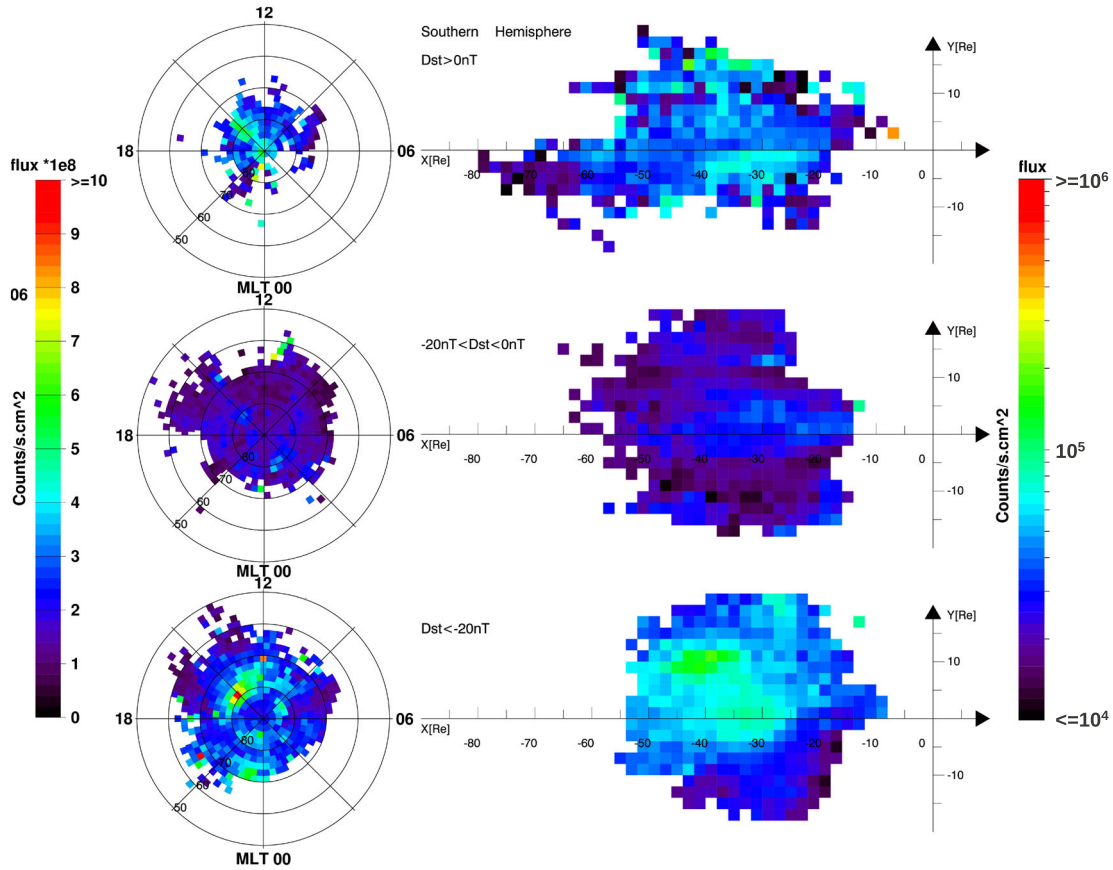


Figure 6. Same as Figure 5, but for Southern Hemisphere. Average transport times from the ionosphere to the plasma sheet are 342, 326, and 252 min for quiet, moderate, and disturbed geomagnetic disturbance levels, respectively.

4.3. IMF Influence and Dawn-Dusk Asymmetry

[51] In order to investigate the role of the interplanetary magnetic field direction on the transport, we sorted the data into four bins according to the IMF clock angle. Each bin contains data from a 90° sector centered around 0° , 90° , 180° , and 270° clock angles.

[52] Since the data are not continuous in time, any effect of the IMF history or any magnetic field or convection

changes during the transport time cannot be investigated. The IMF direction used in the following is the prevailing direction at the time of each observation.

[53] Figure 7 shows the corresponding maps for the four clock angle sectors. Left panels show Northern Hemisphere maps and right panels show Southern Hemisphere maps.

[54] Northward IMF is typically associated with low or stagnant convection and low geomagnetic activity, whereas a

Table 1. Characteristics of the *Engwall et al. [2009a]* data set for different geomagnetic activity levels for Northern and Southern Hemispheres, respectively^a

		A	B	C	D	E	F	G	H	I	J
		Averaged							Convection	Mean	
Activity ^a		AE [nT]	Dst [nT]	Kp	Bx [nT]	By [nT]	Bz [nT]	Pdyn [nPa]	V_{conv}^b [km s ⁻¹]	Travel Time ^c [minutes]	
Northern Hemisphere	Quiet	110.9	8.9	1	2.6	-3.3	0.0	3.1	4.0 ± 0.25	243 ± 49	
	Moderate	199.5	-11.5	2 ⁻	0.8	-2.0	-0.5	1.8	5.0 ± 0.25	204 ± 47	
	Disturbed	444.7	-42.9	3	-0.7	2.1	-1.2	2.3	8.5 ± 0.25	156 ± 41	
Southern Hemisphere	Quiet	162.8	4.4	2 ⁻	-1.2	1.6	0.7	2.7	4.0 ± 0.25	342 ± 53	
	Moderate	232.9	-11.0	2 ⁻	-0.6	1.0	-0.7	1.7	4.5 ± 0.25	326 ± 75	
	Disturbed	411.1	-43.0	3 ⁻	-2.5	1.8	-0.4	2.0	8.0 ± 0.25	252 ± 65	

^aGeomagnetic activity level: Quiet = Dst ≥ 0 nT; Moderate = Dst values in the range 0 to -20 nT; Disturbed = Dst values below -20nT.

^bConvection velocity (statistical mode of distributions in Figure 3).

^cMean travel time of ions from ionosphere to plasma sheet. Error bounds are standard derivation.

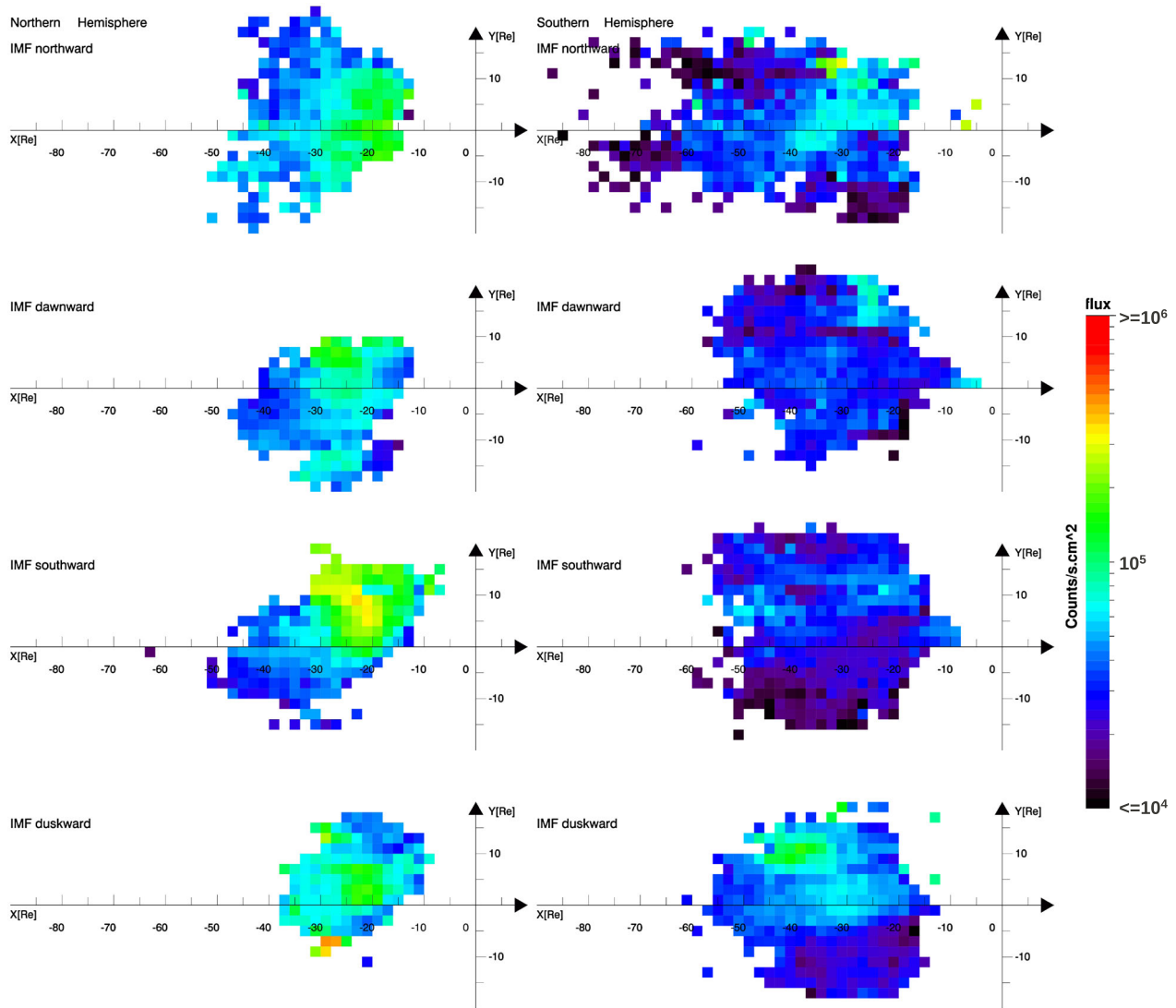


Figure 7. Maps of cold ion feed to the plasma sheet for different IMF orientations. (Left) Northern Hemisphere and (Right) Southern Hemisphere results.

southward directed IMF is associated with high geomagnetic activity level and high convection. One would therefore expect to see some of the same patterns as discussed in section 4.2 and Figures 5 and 6.

[55] For northward IMF, both the maps for Northern and Southern Hemispheres suggest that the cold ions are distributed further downtail (more pronounced in the Southern Hemisphere map). Due to the long transport times, however, it is likely that the IMF orientation and thus the convection and magnetic topology change during the time it takes for the ion to travel from the spacecraft to the plasma sheet.

[56] One interesting feature is apparent from Figure 7, however: There seems to be a persistent dawn-dusk asymmetry, with generally higher supply of ions to the dusk side. Presently, we do not have a good explanation for this observed asymmetry. However, *Howarth and Yau* [2008] used Akebono data to investigate the influence of IMF direction on transport of thermal ions from the polar cap to the

magnetotail. Their results indicated that ions were preferentially fed to the dusk sector of the plasma sheet when the IMF was oriented duskward and to be more evenly distributed when IMF was downward. They also found that a larger fraction of O^+ ions originating from the noon or dusk sectors of the polar cap was deposited in the magnetosphere compared with ions from the dawn or midnight sectors. They attributed their results to higher centrifugal acceleration associated with the larger magnetic field curvature near noon and the larger convection electric field in the dusk sector.

[57] The dawn-dusk asymmetry has also been explained by an asymmetry, in the source region: The evening sector (dusk) thermosphere has been heated during the day and thus reaches higher altitudes. Both neutral and ionized particles in the dusk sector thus have a higher thermal velocity and higher probability for escaping the Earth's gravity field. There is no clear evidence for such a source asymmetry in the maps of *Li et al.* [2012], though.

[58] The IMF orientation, in particular IMF B_y , is also known to cause asymmetries in the magnetotail [e.g., Fairfield, 1979; Cowley, 1981]. Liao *et al.* [2010] studied O^+ outflow from the cusp region and noted the dawn-dusk asymmetry opposite in the two hemispheres and modulated by IMF B_y . Likewise, Noda *et al.* [2003] using Cluster EDI data found correlation between the dayside reconnection electric field orientation and dawn-dusk asymmetries in the magnetospheric convection.

[59] Presumably, IMF B_y penetration is also present in our data set, but since the amount of records with IMF $+B_y$ and IMF $-B_y$ and their magnitudes are roughly similar (average B_y values are around ± 5 nT), this alone cannot explain the persistent asymmetry observed in our data. Neither 4° aberration of the tail can explain since it is smaller than the asymmetry.

5. Summary

[60] We have investigated the transport of cold ions between the polar cap ionosphere and the plasma sheet. The investigation is based on a comprehensive set of measurements of cold ions (predominantly protons with energies 0–70 eV) obtained from the Cluster spacecraft in the high altitude polar cap and lobe regions. As already demonstrated in a preceding paper [Li *et al.*, 2012], the source of the cold ions are primarily the polar cap regions of the ionosphere.

[61] By combining the measurements with a realistic, parameterized magnetic field model [Tsyganenko, 2002a, 2002b], we used guiding center tracing including relevant forces to determine the trajectory of each individual observation.

[62] The outcome of the investigation can be summarized as follows:

[63] 1. The transport of cold ions from the ionosphere to the Earth's nightside plasma sheet is mainly controlled by the convection and the magnetic topology.

[64] 2. During disturbed periods, typically associated with strong convection, transport times from the ionosphere to the plasma sheet are in the order of 30 min to a few hours. Essentially, all outflowing ions are transported to a region Earthward of $40 R_E$ downtail for Northern Hemisphere and $55 R_E$ for Southern Hemisphere.

[65] 3. During periods with low activity and stagnant or low convection, the total outflow is lower and the outflowing ions are distributed over a larger region further downtail. A significant fraction of the outflowing ions are deposited beyond $40 R_E$ downtail for Northern Hemisphere and $55 R_E$ for Southern Hemisphere.

[66] 4. For approximately 15% of the cases, the outflowing ions could not be traced to the plasma sheet. The majority of these are presumably lost along open lobe field lines into the interplanetary space.

[67] 5. We find a persistent dawn-dusk asymmetry in the deposition, with a larger fraction of ions being transported to the dusk side of the magnetotail. This applies for both duskward and dawnward-oriented IMF. We do not observe such a distinct asymmetry in the source region, so the reason for this asymmetry is unclear.

[68] **Acknowledgment.** Masaki Fujimoto thanks the reviewers for their assistance in evaluating this paper.

References

- André, M., and C. M. Cully (2012), Low-energy ions: A previously hidden solar system particle population, *Geophys. Res. Lett.*, **39**, L03101, doi:10.1029/2011GL050242.
- Axford, W. I. (1968), The polar wind and the terrestrial helium budget, *J. Geophys. Res.*, **73**, 6855–6859, doi:10.1029/JA073i021p06855.
- Baker, K. B., and S. Wing (1989), A new magnetic coordinate system for conjugate studies at high latitudes, *J. Geophys. Res.*, **94**, 9139–9143, doi:10.1029/JA094iA07p09139.
- Banks, P. M., and T. E. Holzer (1968), The polar wind, *J. Geophys. Res.*, **73**, 6846–6854, doi:10.1029/JA073i021p06846.
- Cash, M. D., R. M. Winglee, and E. M. Harnett (2010), Storm time production of ring current ions: Variations in particle energization and injection with ionospheric source region, *J. Geophys. Res.*, **115**, A00J12, doi:10.1029/2010JA015759.
- Chappell, C. R., T. E. Moore, and Jr. J. H. Waite (1987), The ionosphere as a fully adequate source of plasma for the Earth's magnetosphere, *J. Geophys. Res.*, **92**, 5896–5910, doi:10.1029/JA092iA06p05896.
- Cladis, J. B. (1986), Parallel acceleration and transport of ions from polar ionosphere to plasma sheet, *Geophys. Res. Lett.*, **13**, 893–896, doi:10.1029/GL013i009p00893.
- Cowley, S. W. H. (1981), Magnetospheric asymmetries associated with the y-component of the IMF, *Planet. Space Sci.*, **29**, 79–96, doi:10.1016/0032-0633(81)90141-0.
- Cully, C. M. (2007), Electric fields and current sheet structure in magnetospheric plasmas, Ph.D. thesis, University of Colorado at Boulder.
- Cully, C. M., E. F. Donovan, A. W. Yau, and H. J. Oppenorth (2003), Supply of thermal ionospheric ions to the central plasma sheet, *J. Geophys. Res.*, **108**, 1092, doi:10.1029/2002JA009457.
- Ebihara, Y., M. Yamada, S. Watanabe, and M. Ejiri (2006), Fate of outflowing suprathermal oxygen ions that originate in the polar ionosphere, *J. Geophys. Res.*, **111**, A04219, doi:10.1029/2005JA011403.
- Engwall, E., A. I. Eriksson, M. André, I. Dandouras, G. Paschmann, J. Quinn, and K. Torkar (2006), Low-energy (order 10 eV) ion flow in the magnetotail lobes inferred from spacecraft wake observations, *Geophys. Res. Lett.*, **33**, 6110–6114, doi:10.1029/2005GL025179.
- Engwall, E., A. I. Eriksson, C. M. Cully, M. André, R. Torbert, and H. Vaith (2009a), Earth's ionospheric outflow dominated by hidden cold plasma, *Nat. Geosci.*, **2**, 24–27, doi:10.1038/NGeo387.
- Engwall, E., A. I. Eriksson, C. M. Cully, M. André, P. A. Puhl-Quinn, H. Vaith, and R. Torbert (2009b), Survey of cold ionospheric outflows in the magnetotail, *Ann. Geophys.*, **27**, 3185–3201.
- Eriksson, A. I., et al. (2006), Electric field measurements on Cluster: Comparing the double-probe and electron drift techniques, *Ann. Geophys.*, **24**, 275–289, doi:10.5194/angeo-24-275-2006.
- Escoubet, C. P., A. Pedersen, R. Schmidt, and P. A. Lindqvist (1997), Density in the magnetosphere inferred from ISEE 1 spacecraft potential, *J. Geophys. Res.*, **102**, 17,595–17,610, doi:10.1029/97JA00290.
- Fairfield, D. H. (1979), On the average configuration of the geomagnetic tail, *J. Geophys. Res.*, **84**, 1950–1958, doi:10.1029/JA084iA05p01950.
- Fairfield, D. H., S. Wing, P. T. Newell, J. M. Ruohoniemi, J. T. Gosling, and R. M. Skoug (2008), Polar rain gradients and field-aligned polar cap potentials, *J. Geophys. Res.*, **113**, A10203, doi:10.1029/2008JA013437.
- Förster, M., G. Paschmann, S. E. Haaland, J. M. Quinn, R. B. Torbert, H. Vaith, and C. A. Kletzing (2007), High-latitude plasma convection from Cluster EDI: Variances and solar wind correlation, *Ann. Geophys.*, **25**, 1691–1707.
- Gustafsson, G., et al. (2001), First results of electric field and density observations by Cluster EFW based on initial months of operation, *Ann. Geophys.*, **19**, 1219–1240.
- Haaland, S., M. Förster, and G. Paschmann (2007), High-latitude plasma convection from Cluster EDI measurements: Method and IMF-dependence, *Ann. Geophys.*, **25**, 239–253.
- Haaland, S., G. Paschmann, M. Förster, J. Quinn, R. Torbert, H. Vaith, P. Puhl-Quinn, and C. Kletzing (2008), Plasma convection in the magnetotail lobes: Statistical results from Cluster EDI measurements, *Ann. Geophys.*, **26**, 2371–2382.
- Haaland, S., et al. (2012a), Estimating the capture and loss of cold plasma from ionospheric outflow, *J. Geophys. Res.*, **117**, A07311, doi:10.1029/2012JA017679.
- Haaland, S., et al. (2012b), Cold ion outflow as a source of plasma for the magnetosphere, in *Dynamics of the Earth's Radiation Belts and Inner Magnetosphere*, *Geophys. Monogr. Ser.*, vol. 199, edited by D. Summers, I. R. Mann, D. N. Baker, and M. Schulz, pp. 341–353, AGU, Washington, D. C., doi:10.1029/2012GM001317.
- Horwitz, J. L., C. J. Pollock, T. E. Moore, W. K. Peterson, J. L. Burch, J. D. Winningham, J. D. Craven, L. A. Frank, and A. Persoon (1992), The polar cap environment of outflowing O^+ , *J. Geophys. Res.*, **97**, 8361–8379, doi:10.1029/92JA00147.

- Howarth, A., and A. W. Yau (2008), The effects of IMF and convection on thermal ion outflow in magnetosphere-ionosphere coupling, *J. Geophys. Res.*, **70**, 2132–2143, doi:10.1016/j.jastp.2008.08.008.
- King, J. H., and N. E. Papitashvili (2005), Solar wind spatial scales in and comparisons of hourly Wind and ACE plasma and magnetic field data, *J. Geophys. Res.*, **110**, A02104, doi:10.1029/2004JA010649.
- Kistler, L. M., C. G. Mouikis, B. Klecker, and I. Dandouras (2010), Cusp as a source for oxygen in the plasma sheet during geomagnetic storms, *J. Geophys. Res.*, **115**, A03209, doi:10.1029/2009JA014838.
- Kozyra, J. U. (1989), Sources and losses of ring current ions: An update, *Adv. Space Res.*, **9**, 171–182, doi:10.1016/0273-1177(89)90326-8.
- Laakso, H., et al. (1997), Electron density distribution in the magnetosphere, in *Correlated Phenomena at the Sun, in the Heliosphere and in Geospace*, vol. 415, edited by A. Wilson, p. 53, ESA Special Publication, Noordwijk, The Netherlands.
- Li, K., et al. (2012), On the ionospheric source region of cold ion outflow, *Geophys. Res. Lett.*, **39**, L18102, doi:10.1029/2012GL053297.
- Liao, J., L. M. Kistler, C. G. Mouikis, B. Klecker, I. Dandouras, and J.-C. Zhang (2010), Statistical study of O⁺ transport from the cusp to the lobes with Cluster CODIF data, *J. Geophys. Res.*, **115**, A00J15, doi:10.1029/2010JA015613.
- Lockwood, M., Jr. J. H. Waite, T. E. Moore, C. R. Chappell, and M. O. Chandler (1985), The cleft ion fountain, *J. Geophys. Res.*, **90**, 9736–9748, doi:10.1029/JA090iA10p09736.
- Lybekk, B., A. Pedersen, S. Haaland, K. Svenes, A. N. Fazakerley, A. Masson, M. G. G. T. Taylor, and J.-G. Trotignon (2012), Solar cycle variations of the Cluster spacecraft potential and its use for electron density estimations, *J. Geophys. Res.*, **117**, A01217, doi:10.1029/2011JA016969.
- Moore, T. E., and J. L. Horwitz (2007), Stellar ablation of planetary atmospheres, *Rev. Geophys.*, **45**, RG3002, doi:10.1029/2005RG000194.
- Moore, T. E., et al. (1995), The thermal ion dynamics experiment and plasma source instrument, *Space Sci. Rev.*, **71**, 409–458, doi:10.1007/BF00751337.
- Moore, T. E., et al. (1997), High-altitude observations of the polar wind, *Science*, **277**, 349–351, doi:10.1126/science.277.5324.349.
- Nilsson, H., et al. (2008), An assessment of the role of the centrifugal acceleration mechanism in high altitude polar cap oxygen ion outflow, *Ann. Geophys.*, **26**, 145–157.
- Nilsson, H., E. Engwall, A. Eriksson, P. A. Puhl-Quinn, and S. Arvelius (2010), Centrifugal acceleration in the magnetotail lobes, *Ann. Geophys.*, **28**, 569–576.
- Noda, H., et al. (2003), Tail lobe convection observed by Cluster/EDI, *J. Geophys. Res.*, **108**, 1288, doi:10.1029/2002JA009669.
- Northrop, T. G. (1963), *The Adiabatic Motion of Charged Particles*, Wiley-Interscience, Hoboken, N.J.
- Paschmann, G., et al. (2001), The electron drift instrument on Cluster: Overview of first results, *Ann. Geophys.*, **19**, 1273–1288.
- Pedersen, A. (1995), Solar and wind magnetosphere plasma diagnostics by spacecraft electrostatic potential measurements, *Ann. Geophys.*, **13**, 118–129, doi:10.1007/s00585-995-0118-8.
- Pedersen, A., et al. (2001), Four-point high time resolution information on electron densities by the electric field experiments (EFW) on Cluster, *Ann. Geophys.*, **19**, 1483–1489, doi:10.5194/angeo-19-1483-2001.
- Pedersen, A., et al. (2008), Electron density estimations derived from spacecraft potential measurements on Cluster in tenuous plasma regions, *J. Geophys. Res.*, **113**, A07S33, doi:10.1029/2007JA012636.
- Riedler, W., et al. (1997), Active spacecraft potential control, *Space Sci. Rev.*, **79**, 271–302, doi:10.1023/A:1004921614592.
- Riedler, W., et al. (1998), Experiment RON for active control of spacecraft electric potential, *Cosmic Res.*, **36**, 49.
- Schmidt, R., et al. (1995), Results from active spacecraft potential control on the Geotail spacecraft, *J. Geophys. Res.*, **100**, 17,253–17,260, doi:10.1029/95JA01552.
- Scudder, J. D., X. Cao, and F. S. Mozer (2000), Photoemission current-spacecraft voltage relation: Key to routine, quantitative low-energy plasma measurements, *J. Geophys. Res.*, **105**, 21,281–22,942, doi:10.1029/1999JA900423.
- Seki, K., et al. (2003), Cold ions in the hot plasma sheet of Earth's magnetotail, *Nature*, **422**, 589–592.
- Su, Y.-J., J. L. Horwitz, T. E. Moore, B. L. Giles, M. O. Chandler, P. D. Craven, M. Hirahara, and C. J. Pollock (1998a), Polar wind survey with the thermal ion dynamics experiment/plasma source instrument suite aboard POLAR, *J. Geophys. Res.*, **1032**, 29,305–29,338, doi:10.1029/98JA02662.
- Su, Y.-J., J. L. Horwitz, G. R. Wilson, P. G. Richards, D. G. Brown, and C. W. Ho (1998b), Self-consistent simulation of the photoelectron-driven polar wind from 120 km to 9 R_E altitude, *J. Geophys. Res.*, **103**, 2279–2296, doi:10.1029/97JA03085.
- Torkar, K., et al. (1999), Spacecraft potential control aboard Equator-S as a test for Cluster-II, *Ann. Geophys.*, **17**, 1582–1591, doi:10.1007/s00585-999-1582-3.
- Torkar, K., et al. (2001), Active spacecraft potential control for Cluster – implementation and first results, *Ann. Geophys.*, **19**, 1289–1302.
- Tsyganenko, N. A. (2002a), A model of the near magnetosphere with a dawn-dusk asymmetry: 1. Mathematical structure, *J. Geophys. Res.*, **107**, 1179, doi:10.1029/2001JA000219.
- Tsyganenko, N. A. (2002b), A model of the near magnetosphere with a dawn-dusk asymmetry: 2. Parameterization and fitting to observations, *J. Geophys. Res.*, **107**, 1176, doi:10.1029/2001JA000220.
- Wilson, G. R., G. Khazanov, and J. L. Horwitz (1997), Achieving zero current for polar wind outflow on open flux tubes subjected to large photoelectron fluxes, *Geophys. Res. Lett.*, **24**, 1183–1186, doi:10.1029/97GL00923.
- Winglee, R. M., and E. Harnett (2011), Influence of heavy ionospheric ions on substorm onset, *J. Geophys. Res.*, **116**, A11212, doi:10.1029/2011JA016447.
- Winningham, J. D., and C. Gurgiolo (1982), DE-2 photoelectron measurements consistent with a large scale parallel electric field over the polar cap, *Geophys. Res. Lett.*, **9**, 977–979, doi:10.1029/GL009i009p00977.
- Yau, A. W., and M. Andre (1997), Sources of ion outflow in the high latitude ionosphere, *Space Sci. Rev.*, **80**, 1–25, doi:10.1023/A:1004947203046.
- Yau, A. W., L. Lenchyshyn, E. G. Shelley, and W. K. Peterson (1985), Energetic auroral and polar ion outflow at DE 1 altitudes: Magnitude, composition, magnetic activity dependence, and long-term variations, *J. Geophys. Res.*, **90**, 8417–8432, doi:10.1029/JA090iA09p08417.